LASER DRILLING OF A SUPERALLOY COATED WITH CERAMIC

P. FORGET*, M. JEANDIN*, P. LECHERVY** and D. VARELA**

 * Ecole des Mines de Paris, Centre des Matériaux P.M. Fourt
   BP 87, 91003 EVRY CEDEX, FRANCE
** SNECMA, Centre de Villaroche, 77550 MOISSY-CRAMAYEL, FRANCE

Abstract

Laser drilling has been developed in advanced aircraft industry in particular to achieve the intricate hole network of the combustion chamber because of several advantages compared to the main competing process, that of electron beam drilling. The combustion chambers for the next generation of engines will be protected on the inner side by a thermal barrier coating (TBC), capable of working at higher temperatures 100-150°C higher, thus improving the gas turbine efficiency.

Consequently, three questions might arise :
- Which was the main phenomena involving material under irradiation during laser drilling ?
- How could these phenomena be described by models ?
- Could laser drilling be applied to multi-layered materials such as a superalloy coated with a TBC ?

An attempt, in part, to answer these questions was made by the study of laser drilling of 1.5 mm thick Hastelloy X sheet coated with conventional plasma-sprayed MCrAlY bond coat plus plasma-sprayed zirconia.

The study focused on microstructural SEM (Scanning Electron Microscopy) observation coupled with modeling. SEM observations, applied to polished (and, if necessary, etched) axial sections of the holes and to edges of the holes, allowed accurate measurements of relevant microstructural parameters which validated the models. The influences of the principal laser parameters such as pulse length, pulse rate and power density were determined. The nature (metal or ceramic) of the side of the part exposed to the beam, the locus of the beam focus and the beam entrance angle were only considered to lesser degree.

Nomenclature

V_i^k, Volume of the ith part (see figure 1) after the kth pulse; H_f^C, H_f^M, Heats of fusion respectively of the ceramic and of the metal; H_v^C, H_v^M Heats of vaporization respectively of the ceramic and of the metal; e_o, Power density; r, Cylindrical coordinate perpendicular to the Oz hole axis; l, Hole mid-depth; τ, Pulse length; ρ, Density; C_p, Specific heat; R, Reflectivity; λ, Thermal conductivity; α, Absorption coefficient; T_f, T_v, Melting and Vaporization temperatures, T_o, Room temperature, φ, ψ, Fractions of respectively melted and evaporated ceramic.

Introduction

The use of lasers is very attractive for drilling small holes at high production rates, as required in the aircraft industry for parts such as nozzle guide vanes and the combustion chamber. The prominent advantages of the process usually claimed are :
- no contact with the part being drilled;
- precise location of the holes;
- no chip problems;
- high production rates;
- large (up to 100 : 1) depth-to-diameter ratios attainable;
- applicable various materials (hard as well as soft);
- achievement of a large range of hole diameters (from about 0.2. μm to about 1.5 mm by percussion drilling, larger by trepanning).

Laser drilling is furthermore promoted by the development of a new generation of systems i.e. the so-called "face-pumped" ("slab") lasers and HSS (high power Solid State) lasers capable of delivering an average power of 1 kW or more (1). Laser drilling has been developed over the past 6 years at the SNECMA Company and is currently applied to the manufacture of air-cooled turbo-engine components such as combustor and turbine parts. A collaborative work between the "Ecole des Mines de Paris" and SNECMA was run to study the expansion of the laser drilling capability to the new ceramic-coated components. The study was conducted in the light of previous works dealing with laser drilling of monolithic materials for applications such as lubrication holes for gears, wire drawing dies, porous ceramic tiles for heat exchanger, small parts in jewellery and air-cooled parts as those involved in this work in aerospace industry (2-6).

Materials and Apparatus

Laser drilling was applied to conventional Hastelloy X sheets coated with ytrria-stabilized zirconia plasma-sprayed onto a MCrAlY bond coat also deposited by conventional air plasma spraying (compositions in table I).

A Nd:YAG rod laser drilling machine integrated into a multi-axis C.N.C. system was used. The main laser drilling parameters are given in table II.

Although the influence of energy, entrance angle and pulse rate were investigated, the work focused on drilling mechanisms occurring for given experimental conditions. All the following observations and calculations reported were made for a pulse length of 240 μs, an energy output of 3.5 J and a given pulse rate. Holes were produced without gas assist by percussion drilling and not in the trepan mode.

Table I - Chemical Compositions of the Alloys, Wt.%.

Substrate	Ni	Cr	Co	Mo	Fe
Hastelloy X	Bal.	22.0	1.5	9.0	18.5
	Mn	Si	C		
	05.	0.5	0.1		
Bond coat	Ni	Cr	Al	Y	Ta
MCRAlY	Bal.	21.0	8.5	0.6	5.7

Table II - Laser Drilling Parameters

Pulse width, μs	0 - 1000
Pulse rate, p.p.s.	$\leqslant 50$
Lens focal length, mm	100 - 150
Beam focus	at work surface
Average output power, W	400

Observation of polished specimens required in certain cases a specific preparation technique to prevent crumbling, cracking and phase transformation (from tetragonal to monoclinic zirconia) in the ceramic layer. It consisted of impregnation under vacuum of the porous material using SHELL EPIKOTE 815 epoxy pre-polymer polymerized by addition of 50% vol. SHELL LINDRITE 15 hardener followed by sectionning and grinding from 1200 grit and then mechanically polishing to 1 μm diamond finish.

Phenomenological Description of Drilling

Energy and Matter Balance

At each pulse, so long as the hole remained blind i.e. for the first 6 shots, the volumes of heated, melted, evaporated, and re-deposited materials correlated with the amount of energy used. For more than 6 pulses, the losses of matter and energy used could not be significantly analyzed partly because some material was expelled from the entrance as well as from the backside of the sheet.

The volumes V_i^k (see the nomenclature) were determined using SEM micrographs of axial sections of the holes. The relative accuracy of the values of the volumes was estimated to be $\pm 10\%$, except thin layers (re-deposited ceramic) for which the accuracy dropped $\pm 20\%$. The main sources of error rested on the assimilation of the various actual shapes to simple shapes (cones, cylinders...) and the determination of the average thicknesses of the layers (figure 1).

The values of the previously mentioned energies were calculated assuming that :
    - the relevant material, i.e. evaporated or melted at a given pulse, was solid before the pulse;
    - the material was heated up to the phase transformation point, temperature remaining constant then;
    - a negligible part of the energy was used to evaporate liquid metal as ascertained by previous work (7, 8) in which it has been shown that most of the material left the worked surface in the liquid state and at relatively high velocity.

The energy requirements for melting and vaporization were calculated using the values of latent heat given in table III. For example, the value of the energy used to melt the ceramic was obtained by multiplying the so-called A coefficient (figure 1) equal to $\rho \left[C_p (T_f - T_o) + H_f^C \right]$ by the volume of material involved. The energies required to evaporate the ceramic and melt the metal were similarly estimated using the so-called B and C coefficients.

555

Table III - Physical Properties of Hastelloy X and Zirconia

Material	ρ(kg.m^{-3})	T_f(°C)	T_v(°C)	H_f(10^4 J.kg^{-1})	H_v(10^4 J.kg^{-1})
Hastelloy X	8220	1250	2400	26.0	-
Zirconia	5200 (solid state)	2700	5000	82.0	1400

	C_p (J.kg^{-1}K^{-1})	λ(W.m^{-1}.K^{-1})	R(at 1.06µm)	α(m^{-1})
Hastelloy X	485 from 0 to 100°C 320 + 0.56 T(K)	9.1 at RT	0.72 up to T_f 1 above T_f	-
Zirconia	502	1.4 10^{-2}	0.4	10^4

Evaporated ceramic was completely removed during the pulse. Re-deposit from the vapor phase was negligible as ascertained by a proper observation of the hole wall. Evaporated metal was also neglected because calculations showed that almost all the unreflected energy (more than 90%) was used to heat Hastelloy X to T_f and to melt it.

			Number of pulses					
			1	2	3	4	5	6
MATTER (10^{-12}m^3)	1:Hole in Hastelloy	V_1^k	87	190	285	390	600	705
	2:Hole in zirconia	V_2^k	0	0	0	0.32	14	45
	4:Remelted Hastelloy	V_4^k	11	10	21	40	$\ll V_1^k$	
	6:Remelted zirconia	V_6^k	0	0	0	0.13	1.9	6.2
	7:Re-deposited zirconia	V_7^k	0	0	0	0.22	5.6	17.5
	6+7:Melted zirconia	$V_6^k+V_7^k$	0	0	0	0.35	7.5	24
	2-7:Evaporated zirconia	$V_2^k-V_7^k$	0	0	0	0.09	8.2	27
ENERGY, E	A.$(V_6^k+V_7^k-V_7^{k-1})$, E to melt zirconia, mJ		0	0	0	4.0	83	205
	B.$(V_6^k-V_7^k-V_7^{k-1})$, E to evaporate zirconia, mJ		0	0	0	8.4	705	1200
	C.$(V_1^k+V_4^k-V_4^{k-1})$, E to melt Hastelloy, J		1.0	1.2	1.2	1.5	2.2	1.6
	Total energy used, J (for à 3.5 J output)		1.0	1.2	1.2	1.5	3.0	3.0

Fig. 1 - Energy-matter balance

With regard to the ceramic when drilling the core of the layer (for example during the 5th and the 6th pulses) half of the energy was used to melt ceramic and half to evaporate it (figure 1).

Hole Depth

The dependence of hole depth on number of pulses was practically linear in drilling Hastelloy X and zirconia. The depth per pulse was, as expected, lower in ceramic than in metal as revealed by the change at the ceramic-metal interface of the representative curve (figure 2). The total number of pulses to drill throughout was too low to show (almost parabolic) decrease of the depth per pulse versus the number of pulses, as can be found when drilling for example thicker materials (9).
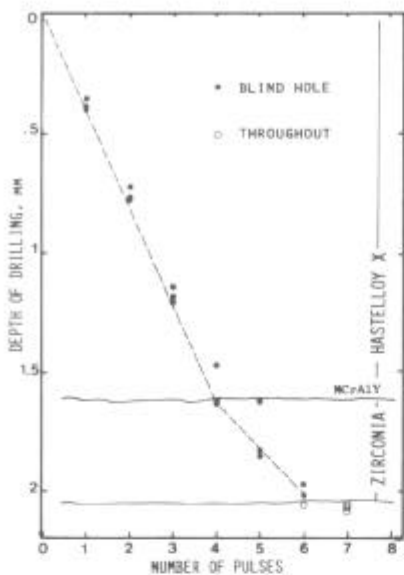
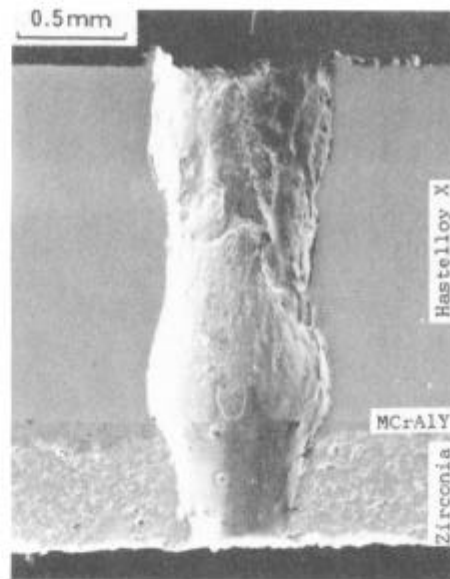Fig.2 - Dependence of the hole depth on number of pulses.

Fig.3 - SEM image of a section of a hole drilled throughout; 3.5 J, 240 µs, 9 pulses.

Hole Shape

Energy Density of the Laser Beam. Starting from the energy conservation law and assuming that radial conduction was negligible and that the profile of the hole followed an isothermal line (generally that of the melting front), the hole shape was the same as that of the energy density distribution of the beam.

The power density which could not be experimentally determined was calculated. The TEM_{00} mode used for drilling gave a Gaussian profile with a power density expressed, in cylindrical coordinates, by

$$e_0(r) = e_{00} \exp\left[-\left(\frac{r}{l}\right)^2\right] \qquad (1)$$

For example for a 2 pulse hole, r at mid-depth (where $e/e_{00} = 1/2$) was measured about 245 µm thus leading to the value of 295 µm for l. Then, e_{00} was given by integrating over the whole pulse duration, i.e.

$$\frac{E}{\tau} = \int_{r=0}^{\infty} \int_{\theta=0}^{2\Pi} e_0(r)\ rdrd\theta \qquad (2)$$

(1) + (2) gave

$$e_{00} = \frac{1}{\Pi} \frac{E}{\tau\ l^2} \qquad (3)$$

which led to the value of $53.3\ 10^9\ W/cm^2$ for e_{00}.

Hole Features. The main features, typical of laser drilling, were (figure 3) :
    - barrelling, due to the presence of a confined hot plasma ("plume") of evaporated material which preferentially eroded the metallic wall of the hole by thermal or pressure effects or made the focus point move within the metal;

557

- taper, due to erosion caused by the expulsion of vaporized or melted material;

- debris, due to resolidified ("recast") or recondensed material and ejected at the lip of the hole;

- recast, made of material, inside and around the hole, which was not completely expelled.

These features were more or less prominent, depending on the drilling conditions. To go into these aspects the reader is referred to other works centered on the effects of laser parameters on hole geometry (10) and how to improve it (11). However, qualitatively, one may say that, during the pulse, the fluidized material was submitted to pressure forces inside the hole from evaporated material and the laser radiation at the absorbing surface. The motion of the material was well revealed by resolidified layers (figure 4).

Craze cracking of ceramic recast due to thermal shock when cooling at the wall and circumferential microcracking at the metal-ceramic interface due to differences between the coefficients of thermal expansion of metal and ceramic also occurred (figure 5).
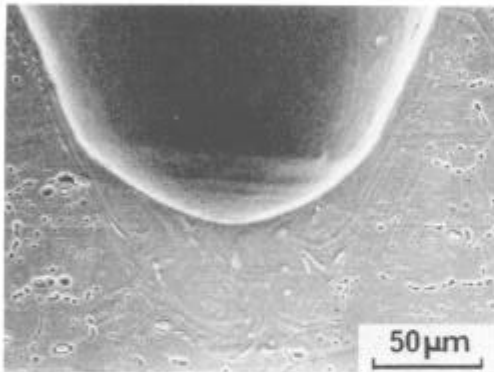
Fig.4 - SEM image of the Hastelloy resolidified layer, etched axial section.
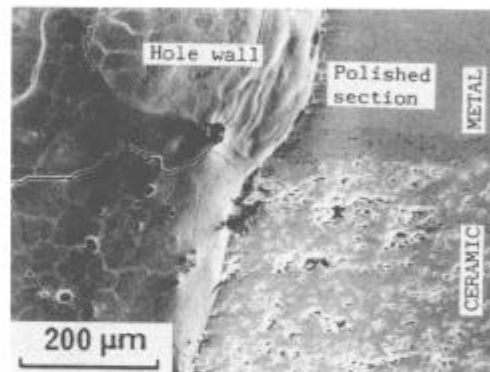
Fig.5 - Craze cracking of zirconia and cracking at the metal/ceramic interface.

Thermal Approach to Drilling

Drilling of Hastelloy X

Axial and radial heat conductions were assumed to be negligible : all the more negligible for the radial because the holes were of a small diameter and for the axial because of the high energy delivered and the short pulses. Moreover, except for the first pulse, axial conduction had no influence on the propagation of the melt front because the energy lost by axial conduction was re-used at the subsequent pulse. For points not on the axis, the previous assumptions were not valid but it did not matter since these points were much less irradiated by the beam.

The energy absorbed by expelling liquid or vaporized material was actually negligible. Lastly, the model did not consider re-focused energy due to multiple internal reflections on the hole wall and involved a reflectivity, R, independent of temperature.

If δv was the volume unit of length d and edges δx, δy at a distance r from the Oz axis and if before the ith pulse the hole surface was located at

$z = z_o(r)$ and at $z_o(r) + d(r)$ after the pulse, the energy needed to drill through a depth $d(r)$ was that used to melt the volume δv that is

$$\int_0^\tau e_o(r)\, \delta x \delta y\, dt = \rho \delta v \left[\frac{1}{1-R} \int_{T_o}^{T_f} C_p\, dT + H_f^M \right] \tag{4}$$

hence

$$d(r) = \frac{\tau\, (1-R)}{\rho} \cdot \frac{e_o(r)}{\displaystyle\int_{T_o}^{T_f} C_p\, dT + H_f^M} \tag{5}$$

with $e_o(r)$ given by the expression (1)

Thus, the depth per pulse along the axis in particular was given by

$$d(0) = \frac{\tau\, (1-R)}{\rho} \cdot \frac{e_{oo}}{\displaystyle\int_{T_o}^{T_f} C_p\, dT + H_f^M} \tag{6}$$

which corresponded numerically to a drilling depth of about 400 μm per pulse, consistent with the experimental results (figure 2) : the reflectivity for Hastelloy X, R, being taken equal to that of nickel, i.e. 0.72.

Drilling of Zirconia

The model. As in the metal, the conduction phenomena were negligible, but in this case because of the low thermal conductivity of the ceramic. Heating involved the bulk of the material mainly due to the transparency of zirconia. Assuming the reflectivity to be constant at solid and liquid states, the power density distribution within the ceramic was expressed as

$$e(r, z) = (1-R)\, e_o(r)\, \exp(-\alpha z) \tag{7}$$

with the hole surface located at z=0 at the pulse origin.
a) For $T < T_f$, the heat conduction equation applied to ceramic was :

$$\lambda \Delta T + Q = \rho\, C_p\, \frac{\partial T}{\partial t} \tag{8}$$

where Q was the heat input in the ceramic given by

$$Q(r, z) = - \frac{de}{dz}(r, z) \tag{9}$$

which, combined with (7), led to

$$Q(r, z) = \alpha(1-R)\, e_o(r)\, \exp(-\alpha z) \tag{10}$$

Although equation (8) was numerically solvable, as in a one-dimensional approach by WAGNER (2) in the case of laser heating of a finite slab, it was analytically considered, assuming the material semi-infinite and no heat losses through the bounding surface for boundary conditions, as ascertained by PAEK et al. (12). This led to a rather complex litteral expression of T.

However, when neglected conduction, relation (8) simplified to

$$Q = \rho \, C_p \, \frac{\partial T}{\partial t} \qquad (11)$$

then,

$$T(r,z,t) = To(r,z) + \frac{1}{\rho C_p} \int_o^t Q(r,z) \, dt \qquad (12)$$

therefore

$$T(r,z,t) = To(r,z) + \frac{\alpha(1-R) \, e_o(r) \, \exp(-\alpha z)}{\rho \, C_p} \cdot t \qquad (13)$$

b) For $T > T_f$, the latent heats of fusion and vaporization were involved, which gave the following new expressions of the heat equation

$$Q(r,z,t) = \rho C_p \, [T(r,z,t) - T_o(r,z)] + \varphi \rho H_f^C + \psi \rho H_v^C \qquad (14)$$

depending on the phenomena involved :

Stage 1; heating of solid ceramic where $T < T_f$, $\varphi = \psi = 0$
Stage 2; melting of ceramic, $T = T_f$, $0 < \varphi < 1$, $\psi = 0$
Stage 3; heating of liquid ceramic, $T_f < T < T_v$, $\varphi = 1$, $\psi = 0$
Stage 4; evaporation of ceramic, $T = T_v$, $\varphi = 1$, $0 < \psi < 1$
Stage 5; heating of evaporated ceramic, $T_v < T$, $\varphi = \psi = 1$.

Then, for Stages 1, 3 and 5 :

$$T(r,z,t) = T_o(r,z) + \frac{1}{C_p} \left[\frac{\alpha(1-R) \, e_o(r) \, \exp(-\alpha z)}{\rho} \cdot t - \varphi H_f^C - \psi H_v^C \right] \qquad (15)$$

for Stage 2 :

$$\varphi(r,z,t) H_f^C = \frac{\alpha(1-R) \, e_o(r) \, \exp(-\alpha z)}{\rho} \cdot t - C_p \, [\, T_f - T_o(r,z) \,] \qquad (16)$$

and for Stage 4 :

$$\psi(r,z,t) H_v^C = \frac{\alpha(1-R) \, e_o(r) \, \exp(-\alpha z)}{\rho} \cdot t - C_p \, [\, T_v - T_o(r,z) \,] - H_f^C \qquad (17)$$

The beam was absorbed at the melting front because liquid ceramic material was expelled during the inter-pulse time, as shown by further results of this work (13).

Consequently, assuming
- the melting front at Stages 1 and 2 and not at 2 and 3;
- room temperature at 0°C and temperature expressed in °C;
- conduction still negligible for short inter-pulse duration (less than 0.2 s), as ascertained by further calculations carried out in the frame of this program but not reported in this article (13);
- z origin at the surface of the ceramic layer for r = 0.

The melting front propagation given by z = d(r,t) was inferred from expression (15) with 0 for r (along the axis) and e_{oo} for e_o

Then,

$$d(0,t) = \frac{1}{\alpha} \left[\ln \left(1 + \frac{\alpha(1-R)e_{oo}}{\rho C_p \, T_f} \cdot t \right) - \ln \left(1 + \frac{H_f^c}{C_p \, T_f} \right) \right] \qquad (18)$$

Experimental Versus Model Results. From relation (18), in the experimental conditions used (see previous sections), the calculated hole depth per shot i.e. $d(0,\tau)$ was about 200 μm which was in keeping with experimental results (see figure 2)

Expressions (15), (16) and (17) set the temperature profile for laser-heated zirconia as function of depth (figure 6). Equivalent depths of melted and evaporated ceramic, respectively $\tilde{z}_f$ and $\tilde{z}_v$ proportional to the volume of melted and evaporated ceramic, were defined as

$$\tilde{z}_f = \int_0^{z_{m,1}} [1 - \psi(0,z,\tau)] \, dz + d(0,\tau) - z_{m,1} + \int_{z_{m,1}}^{z_{m,2}} \varphi(0,z,\tau) \, dz \qquad (19)$$

and

$$\tilde{z}_v = \int_0^{z_{m,1}} \psi(0,z,\tau) \, dz \qquad (20)$$

which numerically gave for $\tilde{z}_f$ and $\tilde{z}_v$ respectively, about 170 μm and 54 μm, thus a fraction of about 0.25 for $\tilde{z}_v/(\tilde{z}_f + \tilde{z}_v)$, which represented the amount of evaporated ceramic. The discrepancy between this calculated value and experimentally estimated volumes ($V_2^5 - V_7^5$ or $V_2^6 - V_7^6$ in figure 1) of about 50% of the affected ceramic was partly attributed to neglecting of solid and liquid materials expelled at the same time as the evaporated.
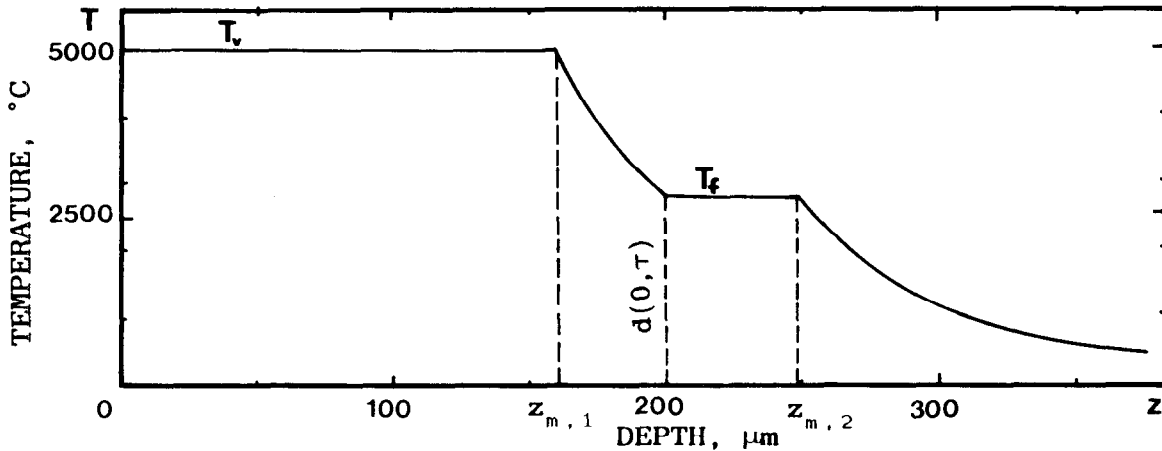

Fig.6 - Temperature profile in the ceramic along the hole axis, at the end of a pulse.

Related Studies

A fluid-mechanics analysis of the removal of melted material was developed and found in good agreement with experimental results. Solidification and cracking (especially at the ceramic-metal interface) phenomena were also investigated. However, all these aspects will be detailed in an additional contribution to be published (13).

Conclusion

The study demonstrated the capability of laser drilling of ceramic-coated superalloys. Thermal models coupled with an energy-matter balance were established. They can be used to predict the main phenomena involving material under irradiation and thus to optimize drilling parameters. They were validated through accurate SEM observations and measurements applied to axial polished section of holes.

Further testing, however like vibrational fatigue testing should be carried out to determine the influence of microcracking at the metal-ceramic interface and the influence of the ceramic layer re-deposited onto the hole wall, which might limit air cooling due to thermal insulation effects.

REFERENCES

1. Anonymous, "Face-Pumped Lasers Enter Industry", Ind. Laser R., (1988),6.

2. D.A. Belforte, "Economic Justification of Industrial Laser Applications", Applications of High Power Lasers, ed. R.R. Jacobs (Bellingham, Wa:SPIE, 1985),18.

3. H.R. Niederhäuser, "Laser Drilling of Wire Drawing Dies", Wire Ind., 53(1986),709.

4. R.W. Frye and D.M. Polk, "Laser Drilling of Ceramic for Heat Exhanger Applications", "Laser Welding Machining and Materials Processing - ICALEO'85, ed. C. Albright, (Berlin, IFS Ltd., 1985),137.

5. A. Laudel, "Laser Machining of Ceramic", (Report BDX-613-2507-UC38, The Bendix Corporation, Kansas City, Mi, 1980).

6. A.G. Corfe, "Laser Drilling of Aero Engine Components", Lasers in Manufacturing, (Krempton, U.K., IFS Ltd., 1983),31.

7. C.M. Adams and G.A. Hardway, "Fundamentals of Laser Beam Machining and Drilling", IEEE Trans. on Ind. and Gen. Appl., 1(1965),90.

8. R.E. Wagner, "Laser Drilling Mechanics", J. of Appl. Physics, 45(1974),4631.

9. W.M. Steen and J.N. Kamalu, "Laser Cutting", Laser Materials Processing, ed. M. Bass, (North-Holland Publ. Co., 1983),15.

10. B.S. Yilbas, "Study of Affecting Parameters in Laser Hole Drilling of Sheet Metals", Trans. of ASME, 109(1987),282.

11. F.R. Joslin, G.E. Palma and G.L. Whitney, "Laser Precision Drilling", U.S. Patent, Request # 875.726.

12. U.C. Paek and F.P. Gagliano, "Thermal Analysis of Laser Drilling, Processes", IEEE J. of Quantum Elec., QE-8(1982),112.

13. P. Forget et al., "Laser Drilling", Adv. Manuf.Proc., To be pub. (1988).